

Dynamical Parameter Estimation using Realistic Photodetection

P. Warszawski, Jay Gambetta, and H. M. Wiseman*
*Centre for Quantum Computer Technology, Centre for Quantum Dynamics,
 School of Science, Griffith University, Brisbane, 4111 Australia.*

We investigate the effect of imperfections in realistic detectors upon the problem of quantum state and parameter estimation by continuous monitoring of an open quantum system. Specifically, we have re-examined the system of a two-level atom with an unknown Rabi frequency introduced by Gambetta and Wiseman [Phys. Rev. A **64**, 042105 (2001)]. We consider only direct photodetection and use the realistic quantum trajectory theory in [P. Warszawski, H.M. Wiseman, and H. Mabuchi, Phys. Rev. A **65**, 023802 (2002)]. The most significant effect comes from a finite bandwidth, corresponding to an uncertainty in the response time of the photodiode. Unless the bandwidth is significantly greater than the Rabi frequency, the observer's ability to obtain information about the unknown Rabi frequency, and about the state of the atom, is severely compromised. This has implications for quantum control in the presence of unknown parameters for realistic detectors, and even for ideal detectors.

PACS numbers: 03.65.Yz, 42.50.Lc, 03.65.Ta, 42.50.Ar

I. INTRODUCTION

In a recent paper, two of us [1], following Mabuchi [2], considered the situation in which an open quantum system with an unknown dynamical parameter is being monitored. Through continuous measurement, information about the unknown parameter is gained. Ref. [1] also focusses on the conditioned state and how the lack of information about the parameter affects its purity. These two papers are part of a small but growing body of work including [3] and [4] (and references therein) that address the problem of reducing *classical* uncertainties in the evolution of quantum systems by performing continuous measurement.

In Ref. [1], the system is taken to be a damped, classically driven two-level atom (TLA) with a driving Hamiltonian ($\propto \hat{\sigma}_x$ in a rotating frame) with an uncertain driving strength Ω . The physical scenario the authors give for this is as follows. An atom is placed in a classical standing wave, thus experiencing a Rabi frequency of

$$\Omega = \Omega_{\max} \sin(kx), \quad (1.1)$$

where k is the wavevector for the classical field and x is the position of centre of mass of the atom. Gambetta and Wiseman then assume that the TLA is equally likely to be placed at any position in the standing wave. Hence, a range of $-\Omega_{\max} \leq \Omega \leq \Omega_{\max}$ exists for the possible driving strength. It is also assumed that the TLA has zero translational motion. This can be justified by assuming that the TLA is fixed by a radio frequency Paul trap or similar confining mechanism [2]. Although it is shown that continual efficient measurement upon the output electromagnetic field of a TLA leads to information gain about the driving strength, the amount

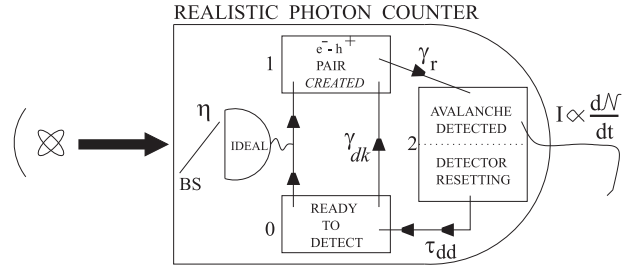


FIG. 1: A schematic illustrating realistic direct detection. The atom is placed at the focus of a parabolic mirror such that that all the fluorescence enters the realistic detector. Realistic photon counting is performed by an avalanche photodiode. The quantum efficiency η of the diode is represented by the the beam-splitter (BS). Single arrowheads within the realistic photodetector indicate Poisson processes. The microscopic detector states are indicated by a 0, 1, and 2.

of information gained depends strongly on the measurement scheme used. The purity of the conditional state also depends strongly on the measurement scheme, but the performance of schemes by these different criteria are *not* well correlated at all [1].

In this paper, we consider only one sort of detection: direct detection. We are interested instead in the difference that it makes when one considers realistic, rather than perfect or ideal detection. As in Ref. [1] we consider the effect on both the rate of information gain and the purity of the conditioned state of the TLA. To treat realistic detection we use the theory developed in Refs. [5, 6, 7]. This generalized the theory of quantum trajectories [8, 9, 10, 11, 12, 13] by determining the state of the system conditioned upon the output of a detector that has dead-time (τ_{dd}), dark counts at rate γ_{dk} , inefficiency η , and finite bandwidth γ_r . A diagram of this detector is displayed in Fig. 1.

The reciprocal of the bandwidth γ_r^{-1} sets the scale for the uncertainty in the delay between the absorption of

*Electronic address: H.Wiseman@griffith.edu.au

photon (which is synonymous with its detection in an ideal detector) and the avalanche of charge which registers this at a macroscopic level in a realistic detector. We find that a finite bandwidth has the greatest effect on our parameter estimation problem. Unless the bandwidth of the detector is substantially greater than Ω_{\max} , the rate of gain of information about Ω is much reduced, and consequently the purity of the system is also. Like the work of Ref. [1] this has important implications for the robustness of quantum feedback control (see for example Refs. [14, 15]).

This paper is structured as follows. In Sec. II we begin with some numerical results to motivate the theoretical developments in the remainder of the paper. In Sec. III we briefly review the theory of parameter estimation based on linear quantum trajectories in Ref. [1], and show how it can be applied to realistic detection. In Sec. IV we use this theory to investigate the evolution of the conditional state for an initially unknown parameter, and in Sec. V we investigate the rate of information gain about the parameter. We conclude with a discussion in Sec. VI.

II. CONDITIONAL PROBABILITY DISTRIBUTION FOR DRIVING STRENGTH

Before providing a theoretical basis, some numerical results are provided to give the reader an insight into the effects of realistic detection on parameter estimation. With an example in mind, the theory contained in the following section should also prove to be more transparent.

We begin by looking at how an observer's probability distribution for the driving strength evolves given a single measurement record (trajectory). Details of the numerical techniques employed to do this will be given at the end of the next section. The distribution is denoted by $P(\Omega|\mathbf{I}_{[0,t]})$, where $\mathbf{I}_{[0,t]}$ represents the measurement record. Obviously, $\mathbf{I}_{[0,t]}$ refers to different events for ideal and realistic detection: it is a record of the times of photodetections and of avalanches, respectively. The initial distribution can be found from Eq. (1.1) with x taken to have a flat distribution. The result is

$$P_0(\Omega) = \frac{1}{\pi\sqrt{\Omega_{\max}^2 - \Omega^2}}. \quad (2.1)$$

The unconditioned evolution of the atom (which is independent of the scheme, or quality, of detection) is given by the master equation (ME)

$$\dot{\rho}(t) = -\frac{i\Omega}{2}[\hat{\sigma}_x, \rho(t)] + \Gamma\mathcal{D}[\hat{\sigma}]\rho(t) = \mathcal{L}_\Omega\rho(t). \quad (2.2)$$

Here Ω is assumed known, Γ is the spontaneous emission rate (which we will set equal to unity), $\hat{\sigma}$ is the atomic lowering operator, and $\hat{\sigma}_x = \hat{\sigma} + \hat{\sigma}^\dagger$. The superoperator \mathcal{D} gives the damping of the system into the environment

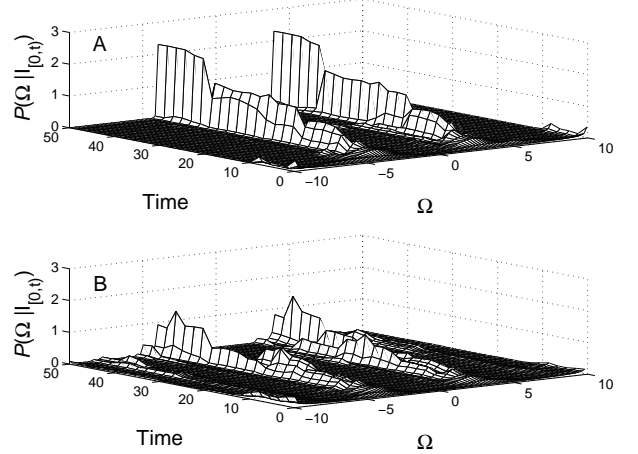


FIG. 2: Plots (A) and (B) show how the probability distribution for Ω typically evolves while continuous direct detection is performed on the output of the quantum system (a TLA inside an optical cavity). Plot (A) is for ideal detection, while (B) is for realistic detection. The parameters used for the photon counter were $\eta = 100\%$, and $\gamma_r = 7\Gamma$, $\tau_{dd} = 0$, $\gamma_{dk} = 0$. The value of Ω used to generate $\mathbf{I}_{[0,t]}$ was $\Omega_{\text{true}} = 4\Gamma$. The maximum allowed value for Ω is $\Omega_{\max} = 10\Gamma$.

and is defined as [16]

$$\mathcal{D}[\hat{a}]\rho = \hat{a}\rho\hat{a}^\dagger - \frac{1}{2}\{\hat{a}^\dagger\hat{a}\rho + \rho\hat{a}^\dagger\hat{a}\}. \quad (2.3)$$

A comparison of ideal and realistic detection is given in Fig. 2. In this figure $\Omega_{\text{true}} = 4\Gamma$, but the observer does not know this, but rather has knowledge described by the prior distribution (2.1) with $\Omega_{\max} = 10\Gamma$. As time goes on, the detection record reveals more about Ω_{true} , and this probability is updated in a Bayesian manner. Note that for both ideal and realistic detectors, the distribution always remains symmetric. This is because the sign of Ω cannot be determined from direct detection. Photoluminescences depend only upon the mean of $\hat{\sigma}_z$, and that is independent of whether the TLA state rotates clockwise or counterclockwise around the $\hat{\sigma}_x$ axis.

In Fig. 2, we have chosen a realistic detector whose only imperfection is a finite bandwidth equal to 7Γ (see figure caption). It can be seen that the degradation of the quality of measurement is quite large even though our 'realistic' detector is well beyond current technology. If we choose the realistic parameters for an APD (avalanche photodiode) used in Refs. [5, 7] we obtain results that are so far from those of ideal detection that a comparison lacks interest.

The fact that the chosen detector parameters give results that are still poor compared to ideal measurement is a little surprising. Very few photodetections are missed under realistic detection with a finite γ_r being the only imperfection. It illustrates that the rate of information gain is very sensitive to an uncertainty in the state of the TLA after a jump.

The plot for realistic detection, Fig. 2 (B), also shows

that it is difficult to distinguish between Ω_{true} and an integer multiple of Ω_{true} , say $m\Omega_{\text{true}}$ (for this figure this occurs only for $|\Omega_{\text{true}}|$ and $2|\Omega_{\text{true}}|$). By Ω_{true} we mean the actual driving strength that exists, but which is initially unknown to the observer. This difficulty exists because the evolution for these two proposed values of the driving strength will place the TLA in the excited state at the same time every integer oscillation (at the smaller frequency). Hence, for certain times there will be a strong correlation between the probabilities of decay. Obviously, a photoemission can still occur when a driving strength of $2|\Omega_{\text{true}}|$ would place the TLA very near ground state, thus ruling out that possible value. Whether these decays that are discriminatory in this sense are detected or not depends on the choice (and duration) of the quantum trajectory in question. In Fig. 2 (B) a small but, persistent (at least up to $t = 50$) probability for $|\Omega| = 2|\Omega_{\text{true}}|$ exists.

It is worth mentioning that the plots in Fig. 2 are based on the ‘same’ photo-absorptions in the ideal and realistic cases. This is possible using the simulation technique of Refs. [7], in which the realistic quantum trajectory can be assured to be consistent with the ideal quantum trajectory.

III. PARAMETER AND STATE ESTIMATION THEORY

We now briefly present the theory of parameter and state estimation in the context that is relevant to this paper. The specific problem that we wish to address involves calculating the new probability distribution for Ω and also obtaining the best estimate of the TLA state, based on the measurement record. Bayesian statistics are required, with the new distribution, based on $\mathbf{I}_{[0,t]}$, given by [17]

$$P(\Omega|\mathbf{I}_{[0,t]}) = \frac{P(\mathbf{I}_{[0,t]}|\Omega)P_0(\Omega)}{\int P(\mathbf{I}_{[0,t]}|\Omega)P_0(\Omega)d\Omega}. \quad (3.1)$$

The best estimate of the TLA state is found from [1]

$$\rho_{\mathbf{I}}(t) = \frac{\int \tilde{\rho}_{\mathbf{I},\Omega}(t)P_0(\Omega)d\Omega}{\int P(\mathbf{I}_{[0,t]}|\Omega)P_0(\Omega)d\Omega}, \quad (3.2)$$

where $\tilde{\rho}_{\mathbf{I},\Omega}(t)$ is the unnormalised state of the TLA given that there was a measurement record $\mathbf{I}_{[0,t]}$ and that the driving strength was Ω .

In this paper we leave the state unnormalised even after jumps, so that

$$\rho_{\mathbf{I},\Omega}(t) = \frac{\tilde{\rho}_{\mathbf{I},\Omega}(t)}{P(\mathbf{I}_{[0,t]}|\Omega)} \quad (3.3)$$

meaning that $P(\mathbf{I}_{[0,t]}|\Omega)$ is actually equal to the norm of the TLA state, when it is evolved with Ω under $\mathbf{I}_{[0,t]}$. Ideally $\mathbf{I}_{[0,t]}$ would be an experimental record, but for

convenience we simulate it using Ω_{true} and then ‘forgetting’ it. The integrals in Eqs. (3.1)–(3.2) require the simulation of the evolution for the entire range of Ω . This means that the process is very time consuming as many trajectories (for the different Ω ’s) have to be run in order to obtain a single trajectory for $P(\Omega|\mathbf{I}_{[0,t]})$ or $\rho_{\mathbf{I}}(t)$.

In order to treat realistic detection, it is necessary to describe not just the state of the TLA, but also the state of a detector (treated classically) which is correlated with the atomic state [5, 6]. We do this by introducing a set of three operators $\rho_{\mathbf{I},s}(t)$ for this supersystem, where here $s = 0, 1, 2$ represents the three classical detector states. These correspond to the ready state ($s = 0$), the avalanching state ($s = 1$) and the resetting state ($s = 2$). Refer to Fig. 1 for details. The state of the TLA is defined as $\rho_{\mathbf{I}}(t) = \rho_{\mathbf{I},0}(t) + \rho_{\mathbf{I},1}(t) + \rho_{\mathbf{I},2}(t)$. Equation (3.2) is trivially generalized to give the best estimate of the supersystem state $\rho_{\mathbf{I},s}(t)$:

$$\rho_{\mathbf{I},s}(t) = \frac{\int \tilde{\rho}_{\mathbf{I},\Omega,s}(t)P_0(\Omega)d\Omega}{\int P(\mathbf{I}_{[0,t]}|\Omega)P_0(\Omega)d\Omega}. \quad (3.4)$$

The three equations, Eqs. (3.1)–(3.2) and Eq. (3.4), are unusable in their present form as $P(\mathbf{I}_{[0,t]}|\Omega)$ and the norm of $\tilde{\rho}_{\mathbf{I},\Omega}(t)$ (which is equal to $P(\mathbf{I}_{[0,t]}|\Omega)$) will become extremely small as t increases. This will be true even for $\Omega = \Omega_{\text{true}}$, as can be seen by considering the probability of a string of measurement results occurring. The probability of a jump in a given infinitesimal interval is never greater than Γdt , so that the norm of the state after m jumps would be less than $(\Gamma dt)^m$ (since the no-jump evolution also decreases the norm of the state). In simulations, a time step of $dt = 10^{-4}\Gamma^{-1}$ is typical. Thus, numerical error introduced by computer round-off necessitates a different approach which we now explain.

A. Linear Quantum Trajectories

In linear quantum trajectories [13], the state is multiplied by a predetermined factor after every measurement event. The normalisation constants are chosen so that the norm of the states corresponding to the most likely values of Ω stay relatively close to unity. Each possible measurement result, r , has an ‘ostensible’ [13] probability, $\Lambda(r)$ associated with it, that we use as the normalising factor. Therefore, we have

$$\bar{\rho}_{\mathbf{I},\Omega,s}(t) = \frac{\tilde{\rho}_{\mathbf{I},\Omega,s}(t)}{\Lambda(\mathbf{I}_{[0,t]})}, \quad (3.5)$$

where $\bar{\rho}_{\mathbf{I},\Omega,s}$ is the supersystem state when linear quantum trajectories are used and $\Lambda(\mathbf{I}_{[0,t]})$ is the ostensible probability for getting $\mathbf{I}_{[0,t]}$,

$$\Lambda(\mathbf{I}_{[0,t]}) = \Lambda(r_k)\Lambda(r_{k-1})\dots\Lambda(r_1). \quad (3.6)$$

Here, we have assumed that the time interval $[0, t]$ has been divided into a very large number, $k = t/dt$, of dis-

crete measurement times. The actual probability of getting $\mathbf{I}_{[0,t)}$, given Ω is

$$P(\mathbf{I}_{[0,t)}|\Omega) = \Lambda(\mathbf{I}_{[0,t)}) \sum_s \text{Tr}[\bar{\rho}_{\mathbf{I},\Omega,s}(t)], \quad (3.7)$$

where the trace is over the TLA and the summation is over the detector states.

This allows Eq. (3.1) and Eq. (3.4) to be written as [1]

$$P(\Omega|\mathbf{I}_{[0,t)}) = \frac{\sum_s \text{Tr}[\bar{\rho}_{\mathbf{I},\Omega,s}(t)] P_0(\Omega)}{\int \sum_s \text{Tr}[\bar{\rho}_{\mathbf{I},\Omega,s}(t)] P_0(\Omega) d\Omega} \quad (3.8)$$

and

$$\rho_{\mathbf{I},s}(t) = \frac{\int \bar{\rho}_{\mathbf{I},\Omega,s}(t) P_0(\Omega) d\Omega}{\int \sum_s \text{Tr}[\bar{\rho}_{\mathbf{I},\Omega,s}(t)] P_0(\Omega) d\Omega}. \quad (3.9)$$

Since $\text{Tr}[\bar{\rho}_{\mathbf{I},\Omega,s}(t)]$ is of order unity for the most likely Ω 's the problems associated with using $\text{Tr}[\bar{\rho}_{\mathbf{I},\Omega,s}(t)]$ have been avoided. The best estimate of the system state allows the conditional evolution of a single stochastic record to be investigated, while $P(\Omega|\mathbf{I}_{[0,t)})$ will allow calculation of the information gain (see following).

In this paper, we choose the ostensible probabilities to be

$$\Lambda(1) = \epsilon dt, \quad (3.10)$$

where $r = 1$ indicates the detection of a photon (ideal detector) or an avalanche (realistic detector). No detection ($r = 0$) has an ostensible probability $\Lambda(0) = 1 - \epsilon dt$. With these ostensible probabilities, the linear quantum trajectory equations for the supersystem describing realistic detection [5, 6] become

$$d\bar{\rho}_0(t) = dt(\mathcal{L}_\Omega - \gamma_{dk} - \eta\Gamma\mathcal{J}[\hat{\sigma}] + \epsilon)\bar{\rho}_0(t) - d\mathcal{N}(t)\bar{\rho}_0(t) + d\mathcal{N}(t)(t - \tau_{dd})\bar{\rho}_2(t) \quad (3.11)$$

$$d\bar{\rho}_1(t) = dt(\mathcal{L}_\Omega - \gamma_r + \epsilon)\bar{\rho}_1(t) + dt(\eta\Gamma\mathcal{J}[\hat{\sigma}] + \gamma_{dk}) \times \bar{\rho}_0(t) - d\mathcal{N}(t)\bar{\rho}_1(t) \quad (3.12)$$

$$d\bar{\rho}_2(t) = dt(\mathcal{L}_\Omega + \epsilon)\bar{\rho}_2(t) + d\mathcal{N}(t)\bar{\rho}_1(t)/\epsilon - d\mathcal{N}(t)(t - \tau_{dd})\bar{\rho}_2(t). \quad (3.13)$$

Here $d\mathcal{N}(t) = 0, 1$, the increment in the number of avalanches, is equivalent to the measurement result r in the time interval $[t, t+dt]$. We maintain the symbol $\mathbf{I}_{[0,t)}$ for the record of avalanches in the interval $[0, t)$, but for clarity we have omitted the subscripts \mathbf{I} and Ω for the $\rho(t)$'s. The superoperator \mathcal{J} is defined by [16]

$$\mathcal{J}[\hat{a}]\rho \equiv \hat{a}\rho\hat{a}^\dagger. \quad (3.14)$$

For simulation purposes we take

$$\epsilon = \eta \frac{\Gamma\Omega_{\text{true}}^2}{2\Omega_{\text{true}}^2 + \Gamma^2}, \quad (3.15)$$

the expected detection rate in steady state (ignoring any dead time) when Ω is known. This is allowed as the

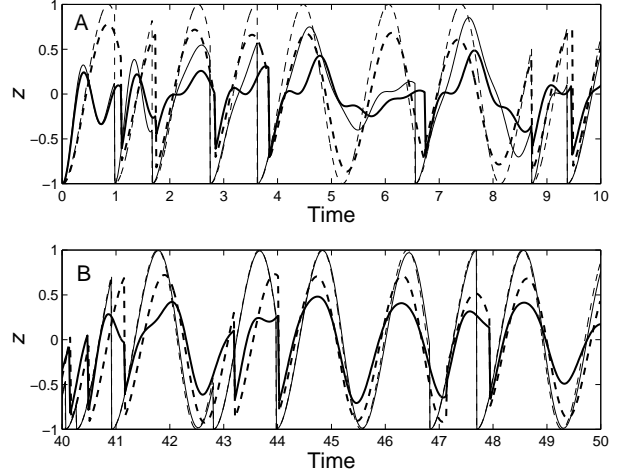


FIG. 3: Two segments of evolution of $z(t)$ in a typical trajectory are shown. The legend is as follows: thin-lines are for ideal detection, thick-lines are for realistic detection, dashed is for known $|\Omega_{\text{true}}|$ and solid is for unknown $|\Omega_{\text{true}}|$. Thus, to be explicit, the thin dashed line is for $|\Omega_{\text{true}}|$ known and ideal detection, the thin solid line is for $|\Omega_{\text{true}}|$ unknown and ideal detection, the thick dashed line is for $|\Omega_{\text{true}}|$ known and realistic detection and, finally, the thick solid line is for $|\Omega_{\text{true}}|$ unknown and realistic detection. The detector and system parameters (and time units) are as for Fig. 2.

results of the simulation are independent of ϵ , thus we are free to choose any value. Note that renormalisation of $\rho(t)$ is occurring even when the detector is resetting and the probability of an avalanche is strictly zero. This illustrates the flexibility of the ostensible probabilities, where the only concern is maintaining a norm of order unity.

IV. CONDITIONAL STATE EVOLUTION

Now that we have explained how the numerical results of Sec. II were obtained, we return to these simulations to investigate the conditional state evolution in a typical realistic quantum trajectory. In Fig. 3 and Fig. 4 we see how $z(t)$ (the mean of $\hat{\sigma}_z$) and the purity of the TLA behaves under a variety of circumstances. Specifically, we consider known $|\Omega_{\text{true}}|$ and ideal detection (thin dashed line), unknown $|\Omega_{\text{true}}|$ (that is, an initial distribution given by Eq. (2.1)) and ideal detection (thin solid line), known $|\Omega_{\text{true}}|$ and realistic detection (thick dashed line) and, finally, unknown $|\Omega_{\text{true}}|$ and realistic detection (thick solid line). The reason why a comparison is made between the trajectories for a TLA randomly placed in the standing wave of the field and trajectories of known $|\Omega_{\text{true}}|$, but unknown sign, is that at $t = \infty$ the sign of Ω_{true} will still not be known, as discussed in Sec. II. This allows us to reveal how far the initially unknown $|\Omega_{\text{true}}|$ trajectories are from their optimal form, given the constraints of direct detection.

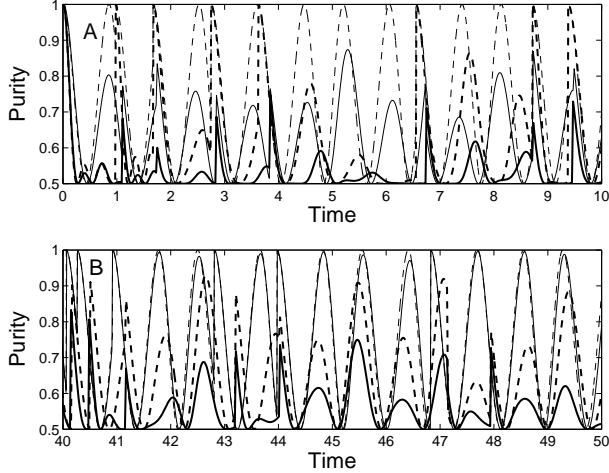


FIG. 4: Here purity is plotted at the same times as $z(t)$ for the same trajectory. The legend and parameters are as for Fig. 3.

The conditioned state corresponding to a known $|\Omega_{\text{true}}|$ is formed from

$$\rho_I(t) = (\rho_{I,\Omega_{\text{true}}}(t) + \rho_{I,-\Omega_{\text{true}}}(t))/2. \quad (4.1)$$

That is, it is an equal mixture of the two conditioned states obtained with a driving strength of $+\Omega_{\text{true}}$ and $-\Omega_{\text{true}}$. Given that we take the TLA as starting in the ground state, these two conditioned states will have the same $z(t)$, but opposite sign for $y(t)$ resulting in $y(t) = 0$ for the mixture as initially $P_0(\Omega)$ is an even mix of positive and negative Ω . If the initial state of the TLA (which is presumed to be known) gives a finite value for $y(t=0)$ then the time of the first jump will give a very small amount of information about $|\Omega_{\text{true}}|$. This is because an early jump would tend to support the conclusion that the TLA had been rotated on the Bloch sphere in the direction that takes it towards the excited state first, while a later jump suggests that the TLA was rotated in the opposite direction. However, the initial state is taken to be the ground state in our simulations. Since for direction detection with no detuning $x(t) = 0$ [8, 16], we have

$$\rho_I(t) = (I + z(t)\hat{\sigma}_z)/2, \quad (4.2)$$

where $z(t)$ could be obtained from either the $+\Omega_{\text{true}}$ or $-\Omega_{\text{true}}$ trajectory. It should now be clear why only $z(t)$ is plotted. In fact, the purity can also be inferred from the $z(t)$ plot as $p_I(t) = (1 + z^2(t))/2$, but a plot is still included for clarity.

As for Fig. 2, the realistic trajectory is forced to be consistent with the ideal trajectory. This is evidenced by the jump times being correlated. Because of the detail of these plots we show two portions of the evolution only, illustrating how improved knowledge over time of the dynamical parameter, Ω , allows closer adhesion to the maximum knowledge trajectory (thin dashed line for

ideal detection and thick dashed line for realistic detection).

In the first $10\Gamma^{-1}$ units of time the frequency of oscillation of $z(t)$ for the realistic detection state (solid black line) is poorly defined. One can also see that the frequency is faster than the true frequency, due to $P_0(\Omega)$ being peaked at $\pm\Omega_{\text{max}}$ [1]. The small amplitude of oscillation is also due to the lack of knowledge about Ω . The range of possible frequencies ensures that when one value of Ω would place the TLA in the excited state, another would place it near the ground state, thus averaging the amplitude of oscillation of $z(t)$ to below unity.

For ideal detection (thin solid line), the frequency of oscillation is also shifting about, but the amplitude of the oscillations have already noticeably increased in size by $t = 10\Gamma^{-1}$. Another feature is that jumps take $z(t)$ to -1 (a pure state) for ideal detection even if $|\Omega_{\text{true}}|$ is not known. This is because there is no time delay in conveying the decay of the TLA to the observer. This is not true for realistic detection where the jump is slightly delayed and the TLA will have rotated out of the ground state by some unknown amount.

The comments of the previous two paragraphs are reflected in the purity for the first $10\Gamma^{-1}$ time units (see figure). The main feature is that with unknown $|\Omega_{\text{true}}|$, the purity of both ideal and realistic detection is well below the maximum possible, except after a detection when it is known that the TLA is in the ground state for ideal detection.

After $40\Gamma^{-1}$ time units, the ideal detection observer has gained enough information about $|\Omega_{\text{true}}|$ that $z(t)$ matches well with the ‘ideal’ $z(t)$ (Fig. 3 (B)). The realistic observer’s $z(t)$ is much closer to the ideal than at the start of the trajectory, but some uncertainty still obviously exists. This is also evidenced by the purity in Fig. 4 (B) where the thin lines now match, but there is a large difference, although less than before, between the thick lines.

V. INFORMATION GAIN

We now move away from conditional dynamics and look at how the ensemble averaged gain of information concerning Ω is affected by realistic detection. As in [1], the measure used to quantify the quality of information gained about Ω is ΔI_I . It is given, in bits, by

$$\Delta I_I = \int d\Omega P(\Omega|\mathbf{I}_{[0,t)}) \log_2 P(\Omega|\mathbf{I}_{[0,t)}) - \int d\Omega P_0(\Omega) \log_2 P_0(\Omega). \quad (5.1)$$

As the distribution for Ω becomes more sharply peaked around $|\Omega_{\text{true}}|$, ΔI_I will increase. Due to the stochastic nature of $\mathbf{I}_{[0,t]}$, an ensemble of trajectories are run in order to obtain the average, ΔI , of ΔI_I that is characteristic of the measurement scheme. Each member of the

ensemble is formed by picking an Ω_{true} randomly (but according to the distribution Eq. (2.1)) and simulating the evolution based on a stochastic trajectory corresponding to that Ω_{true} . A single trajectory for each member of an ensemble of Ω_{true} 's is sufficient as the averaging of the stochasticity is done over the multitude of Ω_{true} 's.

A major difference between parameter estimation for ideal direct detection and realistic direct detection is found when $\Omega_{\text{true}} \gg \Gamma$. We investigate this regime by varying the value of Ω_{max} used in the simulations. This works as the most likely values for Ω_{true} come from close to Ω_{max} . By increasing Ω_{max} we are effectively increasing the values of Ω_{true} used. This method corresponds physically to the TLA being placed randomly in standing waves of different amplitude.

In Fig. 5 (A) the information gain, ΔI , averaged over an ensemble size of 1000 (that is, 1000 different Ω_{true} 's), is shown for ideal detection. The three plots are for $\Omega_{\text{max}} = 5\Gamma, 10\Gamma, 20\Gamma$. In Fig. 5 (B) the results are shown for the same values of Ω_{max} when the monitoring is done with realistic detection. Error bars are included as the ensemble size in this case is only 100, due to the greater computational intensity. As Ω_{max} doubles, the information gain curves for ideal detection are separated by approximately 1 bit at large t . This does not indicate that the detection scheme is more effective at large Ω_{max} , rather, it is an artifact of the initial information content of the distribution $P_0(\Omega)$. This can easily be shown analytically. Consider the integral

$$\int_{-\Omega_{\text{max}}}^{\Omega_{\text{max}}} d\Omega \frac{1}{\pi\sqrt{\Omega_{\text{max}}^2 - \Omega^2}} \log_2 \frac{1}{\pi\sqrt{\Omega_{\text{max}}^2 - \Omega^2}}. \quad (5.2)$$

If the change $\Omega'_{\text{max}} \rightarrow m\Omega_{\text{max}}$ is made, a change of integration variable to $\Omega' = m\Omega$ allows the information of the new distribution to be expressed in terms of the old one. The result is

$$\Delta I_{\mathbf{I},(m\Omega_{\text{max}})} = \Delta I_{\mathbf{I},(\Omega_{\text{max}})} - \log_2 m. \quad (5.3)$$

Thus, every time Ω_{max} is doubled, the initial information decreases by 1 bit. Since the initial information is being subtracted from the information at time t , we can conclude that the width of the $P(\Omega)$ distributions, for different Ω_{max} , in the long time limit are roughly equal for ideal detection.

This is qualitatively different from the case of realistic detection where the information gain for $\Omega_{\text{max}} = 5\Gamma$ and 10Γ are roughly the same and $\Omega_{\text{max}} = 20\Gamma$ sees a significant decrease. Taking into account the fact that as Ω_{max} increases less information is being subtracted away from the information at time t , it is clear that realistic detection is becoming considerably worse at distinguishing between candidates for Ω_{true} . This is more clearly illustrated in Fig. 5 (C) which shows the difference between ideal and realistic detection information gain for the three values of Ω_{max} . We now try to understand these trends by discussing what features of a measurement record allow the information to be accrued.

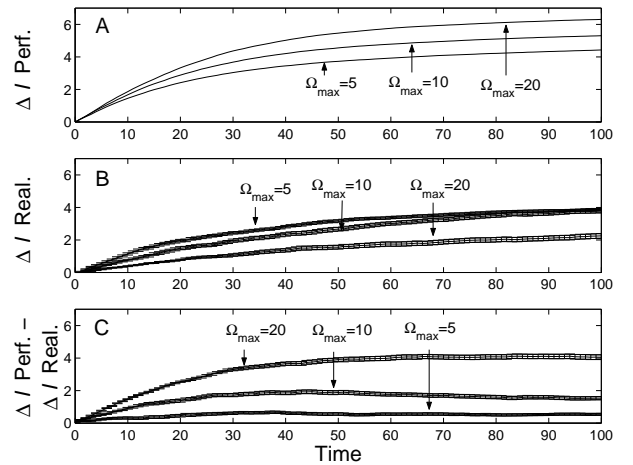


FIG. 5: In plot (A) the ensemble averaged information gain for ideal detection is shown for three different values of Ω_{max} . In plot (B) the ensemble averaged (over 100 trajectories) information gain for ideal detection is shown for the same values of Ω_{max} . In plot (C) the difference between ideal and realistic detection is shown.

The most simple (and naive) way to determine the actual driving strength is to analyse the mean steady-state photon counting rate $\langle \mathbf{I} \rangle_{\text{ss}}$. For ideal direct detection this is

$$\langle \mathbf{I} \rangle_{\text{ss}} = \frac{\Gamma\Omega^2}{2\Omega^2 + \Gamma^2}. \quad (5.4)$$

By using Eq. (5.4) the mean flux can be matched with a particular Ω , given that Γ is known. However, the flux asymptotes to $\Gamma/2$ at large Ω , essentially making one value of Ω indistinguishable from another. Because ideal detection still gives information at large Ω_{max} we deduce that the specific times at which detections are occurring also play a role in determining Ω_{true} .

To consider this effect in more detail we look at the waiting time distribution for photon detections. In perfect direct detection [18]

$$w(\tau) = \frac{\Omega^2}{\Omega^2 - (\Gamma/2)^2} e^{-\Gamma\tau/2} \sin^2\left\{\frac{1}{2}[\Omega^2 - (\Gamma/2)^2]^{1/2}\tau\right\}, \quad (5.5)$$

where $w(\tau)$ is the probability density of a photon being emitted by the TLA at a time τ after the previous emission. The waiting time, $w(\tau)$, is zero at $\tau = 0$ as the TLA is in the ground state after a detection. A plot of this function for $\Omega = 5\Gamma$, with $\Gamma = 1$ is given in Fig. 6 (A). The point that is meant to be taken from this graph is that there are oscillations that make certain emission times more likely (when the TLA is in the excited state) and other times prohibited (when it is in the ground state), given a certain driving strength. These oscillations, which take $w(\tau)$ to zero, are present for all $\Omega > \Gamma/2$, which includes the regime of interest here. This allows the narrowing of the distribution for Ω , based on

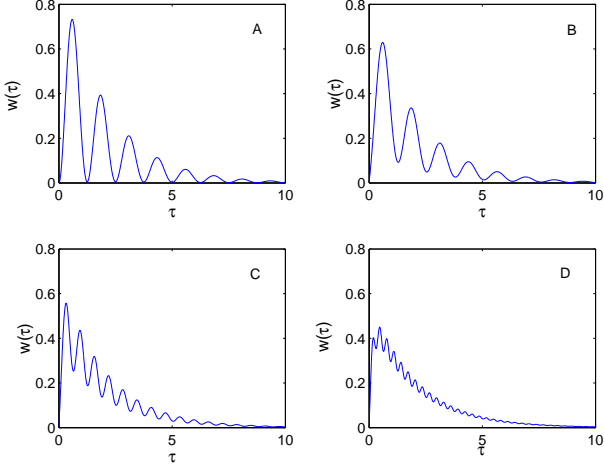


FIG. 6: In plot (A) the waiting time distribution for ideal detection is shown for $\Omega = 5\Gamma$. In plots (B), (C) and (D) the waiting time between avalanches for realistic detection is shown for the values of $\Omega = 5\Gamma$, $\Omega = 10\Gamma$ and $\Omega = 20\Gamma$. The photon counter parameters are as for Fig. 2.

a measurement record, despite the fact that very little information can be obtained from the mean flux rate.

The waiting time distribution for realistic detection is much more complex. In this case, τ would be the waiting time between avalanches of the photodiode, rather than emissions of the TLA. One of the difficulties lies in the fact that there is not a definite state of the atom after an avalanche, due to the finite response time. Thus, initial conditions for the TLA must be chosen as being characteristic of the post-avalanche state. We chose them to be the solution to the ME (2.2) averaged over the time for the avalanche to mature. That is,

$$\rho_{\text{aval.}} = \gamma_r \int_0^\infty e^{-\gamma_r t} \rho(t) dt, \quad (5.6)$$

where $\rho(t)$ is the solution to the ME given that at $t = 0$ the TLA is in the ground state. Of course, this will only be true if the dark counts are ignored, which we will do. The integral in Eq. (5.6) can be carried out analytically with $x = 0$ and the y and z components of the state being

$$y_{\text{aval.}} = \frac{2\Omega(1 + \gamma_r)}{(1 + 3\gamma_r + 2\gamma_r^2 + 2\Omega^2)}, \quad (5.7)$$

$$z_{\text{aval.}} = -\frac{(2\gamma_r + 1)(1 + \gamma_r)}{(1 + 3\gamma_r + 2\gamma_r^2 + 2\Omega^2)}, \quad (5.8)$$

where we have set $\Gamma = 1$.

As the dead time is deterministic, the solutions in Eqs. (5.7)–(5.8) can be evolved forward a time τ_{dd} to give the state of the TLA when the detector becomes ready to detect photons once more. This evolution is done with the ME as the observer is effectively ‘blind’ during the dead time. This gives

$$y_{\text{ready}} = \frac{16\Omega}{S(S^2 + 9)(1 + 3\gamma_r + 2\gamma_r^2 + 2\Omega^2)} \times \left\{ S(1 + 3\gamma_r + 2\Omega^2 + 2\gamma_r^2) - 2 \exp(-3\tau_{\text{dd}}/4) \right. \\ \left. \times [S\gamma_r(\gamma_r - \Omega^2 + 1) \cos(S\tau_{\text{dd}}/4) + (\gamma_r^2 R^2 + \gamma_r - 7\Omega^2) \sin(S\tau_{\text{dd}}/4)] \right\} \quad (5.9)$$

$$z_{\text{ready}} = \frac{-8}{S(S^2 + 9)(1 + 3\gamma_r + 2\gamma_r^2 + 2\Omega^2)} \times \left\{ S(1 + 3\gamma_r + 2\Omega^2 + 2\gamma_r^2) - 2 \exp(-3\tau_{\text{dd}}/4) \right. \\ \left. \times [S\gamma_r\Omega^2(2\gamma_r + 3) \cos(S\tau_{\text{dd}}/4) + \Omega^2(6\gamma_r^2 + 5\gamma_r - 8\Omega^2) \sin(S\tau_{\text{dd}}/4)] \right\}, \quad (5.10)$$

where $S = \sqrt{16\Omega^2 - 1}$ and $R = \sqrt{4\Omega^2 - 1}$.

These solutions are used as initial conditions for the ready state of the detector. A series of 6 linear coupled differential equations must be solved in order to determine $\gamma_r \text{Tr}[\tilde{\rho}_1(\tau)] = w(\tau)_{\text{aval.}}$, which is equal to the probability of an avalanche at time τ (the waiting time). Here, $\tilde{\rho}_1(\tau)$ is the solution to the unnormalised evolution equations given in Eqs. (3.11) and (3.12) with $\epsilon = 0$ and $d\mathcal{N} \equiv 0$ (no avalanches) from τ_{dd} to τ .

The 6 real variables that are necessary are \tilde{y}_0 , \tilde{z}_0 , \tilde{P}_0 , \tilde{y}_1 , \tilde{z}_1 , and \tilde{P}_1 , where the subscripts refer to the detector state and the P 's are the probability of occupation. The variable of interest is $\gamma_r \tilde{P}_1(\tau)$. The equations of motion for these variables are (the reader is reminded that we are assuming $\gamma_{\text{dk}} = 0$ and $\Gamma = 1$)

$$\frac{d}{d\tau} \begin{pmatrix} \tilde{y}_0 \\ \tilde{z}_0 \\ \tilde{y}_1 \\ \tilde{z}_1 \\ \tilde{P}_0 \\ \tilde{P}_1 \end{pmatrix} = \begin{pmatrix} -\frac{1}{2} & 0 & -\Omega & 0 & 0 & 0 \\ 0 & -\frac{1}{2} - \gamma_r & 0 & -\Omega & 0 & 0 \\ \Omega & 0 & -1 + \frac{\eta}{2} & 0 & -1 + \frac{\eta}{2} & 0 \\ 0 & \Omega & -\frac{\eta}{2} & 0 & -\frac{\eta}{2} & -1 \\ 0 & 0 & -\frac{\eta}{2} & 0 & -\frac{\eta}{2} & 0 \\ 0 & 0 & \frac{\eta}{2} & 0 & \frac{\eta}{2} & -\gamma_r \end{pmatrix} \begin{pmatrix} \tilde{y}_0 \\ \tilde{z}_0 \\ \tilde{y}_1 \\ \tilde{z}_1 \\ \tilde{P}_0 \\ \tilde{P}_1 \end{pmatrix}. \quad (5.11)$$

We have solved these equations using MATHEMATICA only for the case of $\eta = 1$, but this is sufficient to illustrate the difference in nature from the waiting time of ideal detection. We have already been using $\eta = 1$ for the numerical simulations shown. The fact that a com-

plete solution for all parameters could not be obtained justifies the numerical solution of Eqs. (3.11)–(3.13) that has been performed. The complicated result for $w(\tau)_{\text{aval.}}$ with $\eta = 1$ and $\tau > \tau_{\text{dd}}$ is

$$w(\tau)_{\text{aval.}} = \frac{4S^2\gamma_r(1+2\Omega^2)(\gamma_r+2\gamma_r^2+2\Omega^2)[\Omega^2+4\gamma_r^3+4\gamma_r^4+S^2\gamma_r^2+\gamma_r(8\Omega^2-1)]^2}{R^2(2\gamma_r-1)T_+T_-U_+U_-} \left(\left\{ 8\Omega(2\Omega-y_{\text{ready}}) \right. \right. \\ \times (\Omega^2+\gamma_r^2-\gamma_r) - 2(2\gamma_r-1)[(2y_{\text{ready}}\Omega-1)(\gamma_r-2\Omega^2)-\gamma_r z_{\text{ready}} R^2] \cos[R(\tau-\tau_{\text{dd}})/2] \\ + R(2z_{\text{ready}}\Omega^2-z_{\text{ready}}\gamma_r-\gamma_r+2\gamma_r y_{\text{ready}}\Omega) \sin[R(\tau-\tau_{\text{dd}})/2] \left. \right\} \exp[-(\tau-\tau_{\text{dd}})/2] \\ - 2R^2[2(1+z_{\text{ready}})\gamma_r^2+\Omega^2-\gamma_r(1+z_{\text{ready}}+2\Omega y_{\text{ready}})] \exp[-\gamma_r(\tau-\tau_{\text{dd}})] \right), \quad (5.12)$$

where y_{ready} , z_{ready} , S , and R are given in, and below, Eqs. (5.9)–(5.10). The expressions T_{\pm} and U_{\pm} are given by

$$T_{\pm} = \gamma_r + 2\gamma_r^2 - \Omega^2 - 4\gamma_r\Omega^2 \pm 3iR\gamma_r^2 \quad (5.13)$$

$$U_{\pm} = 3iS[(2\Omega^2+S^2\gamma_r+16\gamma_r^2\Omega^2-4\gamma_r^2(\gamma_r+1)] \\ \pm S^2[4\gamma_r^2(\gamma_r+3)-2\Omega^2+\gamma_r(5-8\Omega^2)]. \quad (5.14)$$

Note that if $\Omega > 1/2$ then $T_+T_- = |T|^2$ and if $\Omega > 1/4$ then $U_+U_- = -|U|^2$. For $\tau < \tau_{\text{dd}}$, $w(\tau)_{\text{aval.}} = 0$.

Plots of $w(\tau)_{\text{aval.}}$ with $\Omega = 5\Gamma$, 10Γ , and 20Γ are given in Fig. 6 (B), (C) and (D) (with $\tau_{\text{dd}} = 0$). Most notable is that although there are oscillations, they do not take $w_{\text{aval.}}(\tau)$ to zero. The random response time of the photodetector is washing out the peaks and troughs of the ideal detection waiting time distribution, making it much more difficult to distinguish between Ω 's on the basis of the specific times of the avalanches. This effect becomes more pronounced as Ω increases. The relevant characteristic time scale is the response time of the detector. For $\Omega \gtrsim \gamma_r$, the TLA may have rotated out of the ground state significantly by the time the avalanche occurs. If the state of the TLA is smeared out and information contained in the higher order moments of the waiting distribution is lost, then there is no way to determine $|\Omega_{\text{true}}|$ when it is large. This is the reason for the drop-off of the information gain for realistic detection that is seen in Fig. 5.

Although we have done our simulations with a dead time $\tau_{\text{dd}} = 0$, the finite response bandwidth leads to an effective dead time of γ_r^{-1} , which leads to an effective drop in the efficiency of the detector. To rule inefficiency as the cause of the loss of structure in $w(\tau)$ as Ω increases we consider the waiting time distribution for a detector of efficiency η . This is given in Refs. [18] as

$$w(\tau) = \sum_{i=1}^3 \left[\frac{\eta\Gamma\Omega^2(s-s_i)}{2(s_i-s_1)(s_i-s_2)(s_i-s_3)} \right] \Big|_{s=s_i} \\ \times \exp(s_i\tau), \quad (5.15)$$

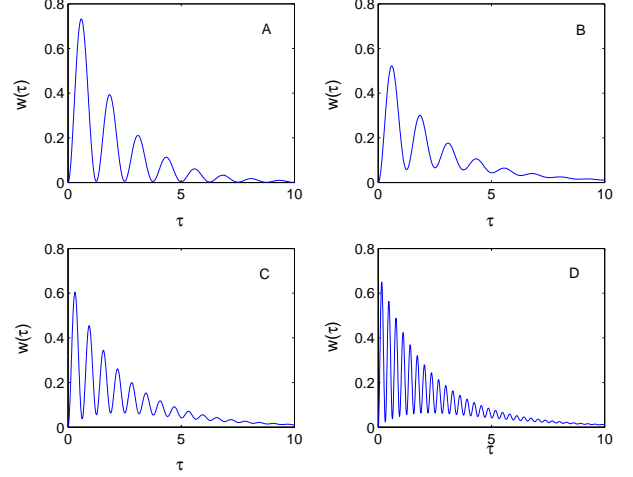


FIG. 7: In plot (A) the waiting time is plotted for $\Omega = 5\Gamma$ and $\eta = 100\%$. In plots (B), (C), and (D) the waiting time is plotted for $\Omega = 5\Gamma$, $\Omega = 10\Gamma$ and $\Omega = 20\Gamma$ and $\eta = 70\%$.

where s_1 , s_2 , and s_3 are the roots of the cubic

$$s(s+\Gamma)(s+\Gamma/2) + \Omega^2(s+\eta\Gamma/2) = 0. \quad (5.16)$$

To illustrate the affect of this waiting time, the roots of this equation where calculated numerically, and plots of $w(\tau)$ with $\Omega = 5\Gamma$, 10Γ , and 20Γ are given in Fig. 7 (B), (C) and (D) (with $\eta = 70\%$) while Fig. 7 (A) is a reproduction of Fig. 6 (A) ($\Omega = 5\Gamma$ and $\eta = 100\%$). Here it is observed that the smearing out of $w(\tau)$ (for detectors with only an inefficiency) is due only to this inefficiency. That is, it is independent of Ω . Thus the smearing out the waiting time distribution as a result of increasing Ω is brought about by the realistic detector (to be more precise the finite bandwidth, γ_r , of the detector).

VI. DISCUSSION

We have investigated the effect of imperfections in realistic detectors upon the problem of quantum state and parameter estimation by continuous monitoring of an open quantum system. Specifically, we have re-examined the system of a two-level atom (TLA) with an unknown driving strength introduced in Ref. [1]. Considering only direct photodetection, we find that the most significant effect comes from a finite bandwidth of the detector. This corresponds to a randomness in the response time of the photodiode (the time from photon absorption to the time when the avalanche reaches a pre-set threshold).

We find that unless the bandwidth is significantly greater than the Rabi frequency, the observer's ability to obtain information about the unknown Rabi frequency, and about the state of the atom, is severely compromised. This is because the waiting time distribution between avalanches is smeared out by the bandwidth, losing the Rabi oscillations that characterize it for an ideal detector. This result shows that the Bayesian update method in Ref. [1] implicitly made use of the structure of the waiting time distribution, rather than simply the mean detection rate. This implies that even for an ideal detector this parameter estimation problem is extremely non-linear, and requires the full power of Bayesian probability theory. Our results thus have implications for quantum control [14] in the presence of unknown parameters even for ideal detectors.

A final comment on the question of the physicality of

the scenario that we have constructed needs to be made. In order to measure the emissions of an atom with an efficiency anywhere close to unity it would be necessary to place the atom in a micro cavity, with the cavity mode being heavily damped so that the atom can be regarded as emitting predominantly into the cavity output beam [19, 20]. However, in this paper we have considered a situation in which the position of the TLA is random, but fixed, across one wavelength of a standing wave field. This has the ramification that the effective decay rate is also position-dependent and hence also uncertain, scaling like the driving strength squared. Thus, in reality, there would be uncertainty in the two dynamical parameters Ω and Γ . In principle, with ideal detection, both these parameters could be found (apart from the sign of Ω) given a long enough measurement record, as the waiting time distribution for ideal detection will be different for different positions of the TLA in the standing wave. It would be an interesting exercise to see how realistic direct detection affects the rate gain of information about Ω and Γ . Another question which would be interesting to answer is, given that homodyne detection of the y quadrature in [1] was shown to provide the greatest gain in information, does this result also apply when realistic detection affects are taken into account.

Acknowledgments

This work was supported by the Australian Research Council.

- [1] J. Gambetta and H.M. Wiseman, Phys. Rev. A **64**, 042105 (2001).
- [2] H. Mabuchi, Quan. Semiclass. Opt. **8**, 1103 (1996).
- [3] A.C. Doherty, S.M. Tan, A.S. Parkins and D.F. Walls, Phys. Rev. A **60**, 2380 (1999).
- [4] F. Verstraete, A.C. Doherty and H. Mabuchi, Phys. Rev. A **64**, 032111 (2001).
- [5] P. Warszawski, H.M. Wiseman, and H. Mabuchi, Phys. Rev. A **65**, 023802 (2002).
- [6] P. Warszawski and H.M. Wiseman, J. Opt. B. **5**, 1 (2003).
- [7] P. Warszawski and H.M. Wiseman, J. Opt. B. **5**, 15 (2003).
- [8] H.J. Carmichael, *An Open Systems Approach to Quantum Optics* (Springer-Verlag, Berlin, 1993).
- [9] V.P. Belavkin and P. Staszewski, Phys. Rev. A **45**, 1347 (1992).
- [10] A. Barchielli, Int. J. Theor. Phys. **32**, 2221 (1993).
- [11] J. Dalibard, Y. Castin and K. Mølmer, Phys. Rev. Lett. **68**, 580 (1992).
- [12] C.W. Gardiner, A.S. Parkins, and P. Zoller, Phys. Rev. A **46**, 4363 (1992).
- [13] H.M. Wiseman, Quantum Semiclass. Opt **8**, 205 (1996).
- [14] A.C. Doherty, S. Habib, K. Jacobs, H. Mabuchi, S.M. Tan, Phys. Rev. A **62**, 012105 (2000).
- [15] H.M. Wiseman, S. Mancini, and J. Wang, Phys. Rev. A **66**, 013807 (2002).
- [16] H.M. Wiseman and G.J. Milburn, Phys. Rev. A **47**, 1652 (1993).
- [17] G.E.P. Box and G.C. Tiao, *Bayesian Inference in Statistical Analysis*, (Addison-Wesley, Sydney 1973).
- [18] H.J. Carmichael, S. Singh, R. Vyas and P.R. Rice, Phys. Rev. A, **39**, 1200 (1989).
- [19] P. R. Rice and H. J. Carmichael, IEEE J. Quantum Elect. **24**, 1351 (1988).
- [20] Q. A. Turchette, R. J. Thompson, and H. J. Kimble, Appl. Phys. B **60**, S1 (1995).